Cancer Immunology, Immunotherapy (2021) 70:391–404
https://doi.org/10.1007/s00262-020-02690-w

ORIGINAL ARTICLE

Evaluation of antitumor immunity by a combination treatment of high-dose irradiation, anti-PDL1, and anti-angiogenic therapy in murine lung tumors

Jenny Ling-Yu Chen[1,2,3] · Chun-Kai Pan[4] · Yu-Sen Huang[1,5] · Ching-Yi Tsai[4,6] · Chun-Wei Wang[1,2] · Yu-Li Lin[4] · Sung-Hsin Kuo[2,3] · Ming-Jium Shieh[7]

Received: 13 December 2019 / Accepted: 31 July 2020 / Published online: 6 August 2020

Abstract

C57BL/6 mice implanted in the flank with murine Lewis lung carcinoma cells were randomized into control, anti-angiogenic, anti-PD-L1, radiotherapy (RT), RT + anti-angiogenic, RT + anti-PD-L1, and RT + anti-PD-L1 + anti-angiogenic therapy groups. Immune response and immunophenotyping were determined by flow cytometry. Vasculature analysis after RT and anti-angiogenic therapy was assessed by quantified power Doppler sonography. Antitumor response, survival, and rechallenged tumor growth were evaluated. RT increased PD-L1 expression on CD8+ T, CD4+ T, dendritic, myeloid-derived suppressor cells (MDSCs), and tumor cells and increased PD-1 expression on CD8+ and CD4+ T cells. Anti-angiogenic therapy insignificantly decreased the RT-induced PD-1 expression on CD8+ and CD4+ T cells, implying a weak reversal of the immune-suppressive environment. Transient vessel collapse was observed within days after RT, and blood flow recovered at 1 week after RT. RT + anti-PD-L1 suppressed the tumor growth, improved survival, and prolonged immune memory capable of protecting against tumor recurrence, evidenced by local accumulation of CD8+ T cells and reduction in MDSCs in microenvironment. Similar and more prominent effects were observed when anti-VEGF was added to RT + anti-PDL1 therapies, implying an additive, rather than synergistic, antitumor immunity. Phenotypic analyses revealed that anti-cancer treatments increased the proportion of effector memory T cells in TILs and splenocytes, and RT, alone or in combination with other treatments, further increased the proportion of central memory T cells in splenocytes. These results provide evidence on operating the immunosuppressive tumor environment and offer insights into the design of the new combination treatment.

Keywords Radiotherapy · Immune response · Anti-angiogenesis · Anti-PD-L1 · Tumor microenvironment · Cancer

Electronic supplementary material The online version of this article (https://doi.org/10.1007/s00262-020-02690-w) contains supplementary material, which is available to authorized users.

✉ Yu-Li Lin
linyuli888@gmail.com

[1] Department of Radiology, National Taiwan University College of Medicine, Taipei, Taiwan

[2] Division of Radiation Oncology, Department of Oncology, National Taiwan University Hospital, Taipei, Taiwan

[3] National Taiwan University Cancer Center, National Taiwan University College of Medicine, Taipei, Taiwan

[4] Department of Medical Research, National Taiwan University Hospital, No. 7, Chung-Shan S. Road, Taipei 100, Taiwan

[5] Department of Medical Imaging, National Taiwan University Hospital, Taipei, Taiwan

[6] Institute of Toxicology, National Taiwan University College of Medicine, Taipei, Taiwan

[7] Institute of Biomedical Engineering, College of Medicine and College of Engineering, National Taiwan University, Taipei, Taiwan

Introduction

Radiotherapy (RT) is widely used in the treatment of primary and metastatic tumors [1]. The biological response of tumors to radiation includes DNA damage, modulation of signal transduction, and alteration of the tumor microenvironment [2]. High-dose ionizing radiation causes tumor cell death, however, local recurrence and metastasis are often observed following irradiation, indicating the inadequacy of RT-induced response to maintain antitumor immunity. Over the past decades, it has become clear that components within the tumor microenvironment, such as the tumor-infiltrating immune cells and the tumor vascular bed, have potential effect on RT efficacy [2, 3]. Moreover, preclinical studies have demonstrated the superiority of hypofractionated ablative doses on the generation of antitumor responses, effectively transforming the tumor microenvironment from one that is immunosuppressive to proimmunogenic, which is more favorable for cancer immunotherapy [4–6]. In clinical practice, high doses of radiation achieved by hypofractionation (40–50 Gy in 4–5 fractions) generated promising results in both early stage lung cancer and oligometastases disease, and have indeed been incorporated in the clinical treatment guidelines [7, 8].

Therapeutic blockade of programmed death-ligand 1 (PD-L1) can enhance the function of effector T cells, however, it might not be useful as an efficacious monotherapy against all tumors [9]. Within the tumor microenvironment, RT induces PD-L1 expression on tumor cells and in the microenvironment, leading to an immunosuppressive mechanism and resistance to anticancer treatment [3, 10]. Targeting the immunosuppressive mechanism via therapeutic blockade of the PD-L1 axis has been demonstrated to be effective in overcoming RT-induced immune resistance, eliciting therapeutic benefits in combination with RT [4, 6, 11–13].

RT also affects the vasculature. Specifically, single high-dose irradiation induces apoptosis and senescence of endothelial cells resulting in tissue hypoxia with the vascular rebound effect as a consequence of growth factor-induced vasculogenesis and angiogenesis, thereby providing opportunities for anti-vascular endothelial growth factor (anti-VEGF) therapeutic intervention in combination with RT [14, 15]. Ablative RT causes transient reduction in, and subsequent recovery of, tumor blood flow [16]. Furthermore, anti-angiogenic therapy preceding RT generates a normalization period during which tumor oxygenation increases, with an enhanced radiation response [17].

In the tumor microenvironment, VEGF plays a central role in suppressing tumor-directed immune responses and promoting angiogenesis [18]. Hence, modulating the VEGF-induced suppressive state in the tumor microenvironment through inhibition of angiogenesis is an attractive complementary strategy for immune checkpoint inhibitors [19]. Anti-angiogenic therapy may enhance anticancer immune responses by normalizing tumor vasculature and reprogramming the tumor microenvironment to an immune-permissive status [20]. Initial studies of the complex relationship between angiogenesis, VEGF signaling, and the immune system suggest that the combination of immune checkpoint blockade with inhibition of angiogenesis has therapeutic potential [21, 22]. In fact, simultaneous immune checkpoint blockade and anti-VEGF therapy demonstrated encouraging antitumor activity and safety in a prospective human clinical trial [23].

Combinations of any two of the following: radio-, immune-, or anti-angiogenic therapies, have reported therapeutic potential for improving treatment outcomes [24]. Based on previously described interactions and synergy, a trimodal approach combining RT with anti-angiogenic therapy and cancer immunotherapy offers an innovative and interesting therapeutic strategy for treatment of cancer [25]. Here, we evaluated the antitumor efficacy of a combination of high-dose irradiation, anti-PD-L1, and anti-angiogenic therapies.

Materials and methods

Mice and cell lines

Six-week-old C57BL/6 mice were purchased from the National Laboratory Animal Center (Taipei, Taiwan). All mice were maintained under specific pathogen-free conditions. The in vivo experimental protocols were approved by the Institutional Animal Care and Use Committee (IACUC 20160399). Lewis lung carcinoma (LLC) cells were purchased from the Food Industry Research and Development Institute (FIRDI, Hsinchu, Taiwan) and were maintained at 37 °C in a humidified atmosphere of 5% CO_2/95% air in DMEM supplemented with 10% heat-inactivated fetal bovine serum and penicillin–streptomycin under sterile tissue culture conditions. All cell lines were cultured to limited passage before implantation.

Antitumor therapy

C57BL/6 mice were implanted subcutaneously with 2×10^5 LLC cells on the flanks [13, 26]. All mice were group-housed (five mice/cage) under a fixed light–dark cycle with access to sterilized food and water ad libitum and were evaluated for signs of deteriorating physical and behavioral health with the assistance of veterinary technicians. LLC cells were allowed to grow, allowing the tumors to become established

9 days after implantation (mean starting volume = 40 mm^3). The tumor-bearing mice were then randomized into seven treatment groups: control, anti-VEGF (100 μg on day 0, 3, 6, 9, total 400 μg), anti-PD-L1 (100 μg on day 1, 4, 7, 10, total 400 μg), RT (40 Gy/4 fx on day 1, 2, 3, 4), RT + anti-VEGF, RT + anti-PD-L1, and RT + anti-PD-L1 + anti-VEGF. Drugs were administered intraperitoneally. Tumor volume and body weight were measured every 3 days for 8 weeks. The tumor volume was calculated as (length × $width^2$)/2. Humane endpoints were determined according to a clinical scoring system based on that outlined in the IACUC of our institution. Animals with a weight loss of 20% or more, tumor diameter larger than 20 mm, tumor causing severely impaired ambulation, or tumor ulceration were euthanized. For tumor rechallenge experiments, mice were implanted on contralateral flanks with 4×10^5 LLC cells on day 40 of experiments. Monoclonal antibodies against mouse PD-L1 (clone 10F.9G2, isotype rat IgG2b kappa) were purchased from Bio-Xcell [27, 28]. Bevacizumab—a recombinant humanized monoclonal antibody against VEGF, is composed of the consensus human IgG1 framework regions and the antigen-binding regions of the murine IgG1 anti-human VEGF monoclonal antibody A.4.6.1, and is cross-reactive with other species including murine xerografts—was used as the anti-VEGF therapy (purchased from Genentech through the National Taiwan University Hospital pharmacy) [29–31]. RT (40 Gy in four fractions) was administered using a GammaCell 40 (Cs-137, 337 cGy/min dose rate, CIS Bio International, Saclay, France), with a custom-made lead shield to deliver RT to one tumor and minimal dose to other areas [32].

Tumor vasculature analysis

To assess tumor vasculature response to RT and anti-VEGF therapy, quantified power Doppler sonography (Prospect T1, S-Sharp Corporation, New Taipei City, Taiwan) was used before RT and on days 0, 3, 6, and 9 post-RT, to assess vasculature response to RT (40 Gy) and anti-VEGF therapy [16]. Ultrasonic contrast imaging was performed by injecting 10 μL of the microbubble agent, USphere Prime (average diameter of 1.2 μm phospholipid-coated microbubbles, Trust Bio Sonics, Zhubei City, Taiwan), to each mouse followed by 0.1 mL normal saline injection. Real-time ultrasound imaging was performed before RT, as well as 3 and 9 days post-RT, to capture microbubble flow paths, and to calculate maximal intensity projection (MIP) for evaluating the path of moving microbubbles with summation over time in the tumor vasculature [33]. Tumors were sonographically imaged using the following scanning parameters: frequency 33–50 MHz, and pulse repetition frequency (PRF) 1–10 kHz.

Tumor-infiltrating lymphocyte (TIL) and splenocyte preparation

To isolate tumor-infiltrating lymphocytes (TIL), solid tumors were excised 10 days after irradiation, single-cell suspensions were processed using a gentleMacs dissociator and a murine tumor dissociation kit (Miltenyi Biotec), followed by density gradient centrifugation on an 80/40% Percoll (GE Healthcare, Piscataway, NJ, USA) gradient. For splenocyte preparation, the spleen was removed 10 days after irradiation and a single cell suspension was prepared by forcing the spleen through a 400 μm stainless steel mesh strainer. Erythrocytes were lysed with hypotonic buffered solution and lymphocytes were washed with Hanks' balanced salt solution prior to being resuspended in RPMI medium supplemented with 10% fetal calf serum.

Flow cytometry and immunophenotyping

Single cell suspensions were prepared from spleens and tumors. Cells were stained with fluorescent-labeled antibodies (BD Biosciences, San Diego, CA, USA) and analyzed by a LSRII flow cytometer (BD Biosciences, San Diego, CA, USA). For analysis, nonspecific binding was blocked and expression levels of CD4, CD8, CD45, CD44, CD62, CD11b, CD11c, Gr1, F4/80, Foxp3, PD-1, and PD-L1 were examined by multiparameter flow cytometry.

Statistical analysis

Statistical analyses were performed using the Statistical Package for Social Sciences for Windows, version 17.0 (SPSS Inc., Chicago, IL, USA). Experiments were repeated at least twice by two independent experiments with an interval of 1 month. Comparisons between experimental groups were assessed using two-tailed unpaired Student's *t* test. Survival data were analyzed by log-rank Mantel–Cox test. p values < 0.05 (*), < 0.01 (**), and < 0.001 (***) were considered statistically significant for comparisons between experimental groups. When Bonferroni correction was applied for multiple comparison (RT, anti-VEGF, anti-PD-L1, either alone or in combination), p-values < 0.01 (**) and < 0.001 (***) were considered statistically significant [34].

Results

Increased PD-L1 and PD-1 expression in the tumor microenvironment following RT

Localized ablative irradiation has been shown to mediate tumor regression; however, relapse often occurs, which

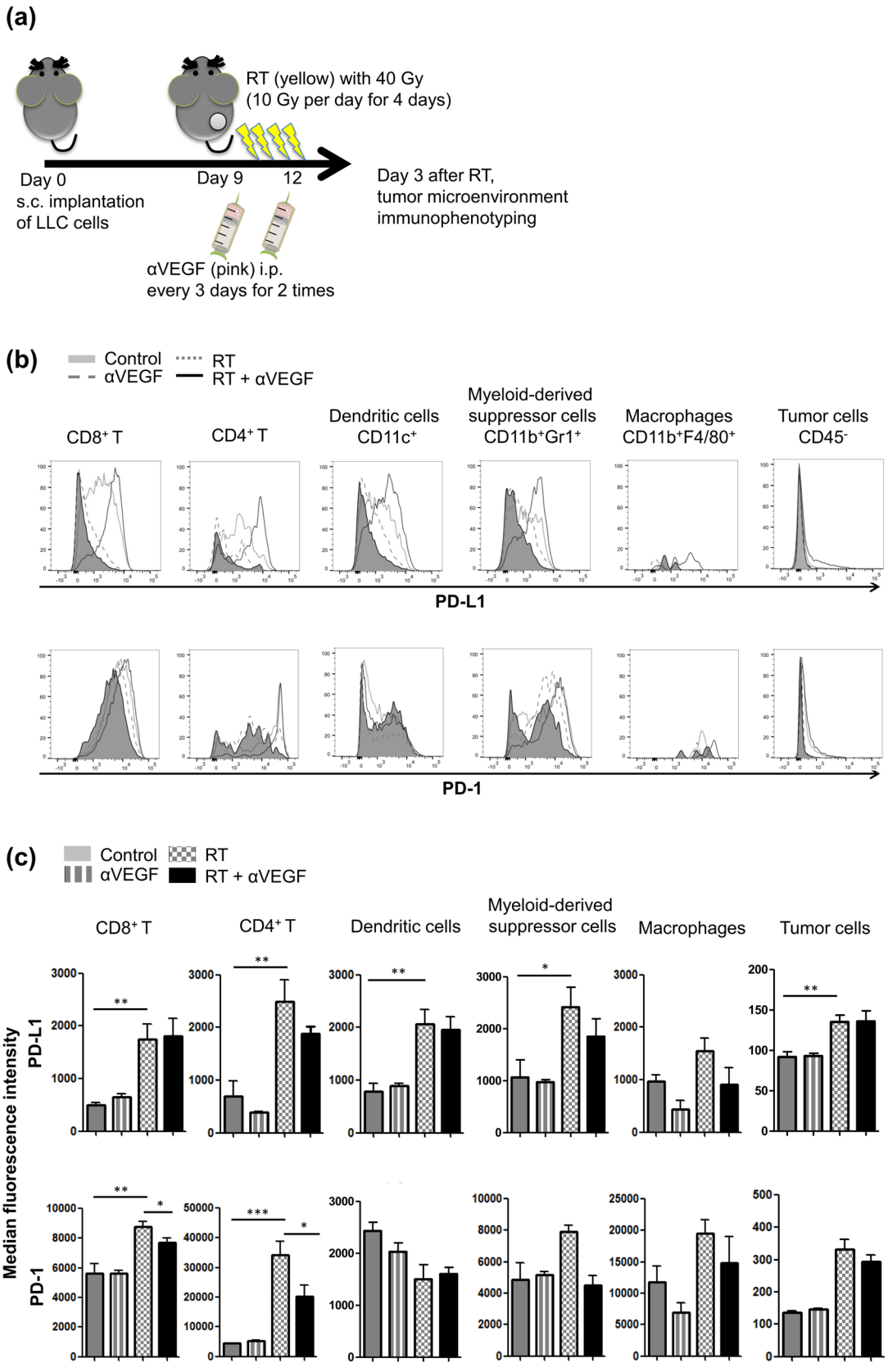
(a)
RT (yellow) with 40 Gy
(10 Gy per day for 4 days)
Day 0
s.c. implantation
of LLC cells
Day 9
12
Day 3 after RT,
tumor microenvironment
immunophenotyping
αVEGF (pink) i.p.
every 3 days for 2 times
(b)
Control
αVEGF
RT
RT + αVEGF
CD8+ T
CD4+ T
Dendritic cells
CD11c+
Myeloid-derived
suppressor cells
CD11b+Gr1+
Macrophages
CD11b+F4/80+
Tumor cells
CD45-
PD-L1
PD-1
(c)
Control
αVEGF
RT
RT + αVEGF
CD8+ T
CD4+ T
Dendritic cells
Myeloid-derived
suppressor cells
Macrophages
Tumor cells
Median fluorescence intensity
PD-L1
PD-1

◂**Fig. 1** PD-L1 and PD-1 expression profiles in tumor microenvironments after radiotherapy (RT) and anti-VEGF therapy. **a** C57BL/6 mice were subcutaneously injected into the flank with 2×10^5 LLC cells. Once the tumor was established, mice were locally treated with 10-Gy dose/fraction of RT, one fraction per day, for 4 days, to a total dose of 40 Gy, and 100 μg anti-VEGF was administered intraperitoneally every 3 days for a total of two times. Three days after RT treatment, tumors were removed and digested into single-cell suspensions, which were blocked with anti-FcR mAbs and then subjected to surface staining. Representative flow cytometric data (**b**) and median fluorescence intensity histograms (**c**, means ± SEM) for PD-1 and PD-L1 expression on CD8+ and CD4+ T cells, dendritic cells (CD11c+), myeloid-derived suppressor cells (MDSCs, CD11b+Gr1+), macrophages (CD11b+F4/80+), and tumor cells (CD45−). $*p<0.05$, $**p<0.01$, and $***p<0.001$. Experimental groups contained five mice per group. Studies were conducted twice in two independent experiments with an interval of 1 month, and the presented histograms (**c**) are the combined data of the two independent experiments

may be partly due to radiation-induced adaptive immunity resulting from engagement of T cell negative regulatory pathways, such as the PD-L1/PD-1 axis. LLC cells were implanted subcutaneously on the flanks of mice, and the tumor-bearing animals were then treated with high-dose ablative irradiation of 40 Gy in four fractions (one fraction per day) for 4 days. Thereafter, we examined the expression of PD-1 and PD-L1 on tumor cells and in the microenvironment on day 3 after irradiation (Fig. 1a). High-dose ablative irradiation increased PD-L1 expression on CD8+ T cells ($p=0.002$), CD4+ T cells ($p=0.003$), dendritic cells (DC, CD11c+, $p=0.001$), myeloid-derived suppressor cells (MDSCs, CD11b+Gr1+, $p=0.018$), and tumor cells (CD45–, $p=0.002$), and increased PD-1 expression on CD8+ ($p=0.001$) and CD4+ T cells ($p<0.001$) (Fig. 1b, c). Hence, radiotherapy-induced increase in the PD-L1/PD-1 axis in the tumor microenvironment may inhibit T cell function and result in tumor relapse, an important mechanism for acquired radioresistance in tumors.

Effects of combinatorial anti-VEGF therapy on RT-induced PD-L1 and PD-1 expression in the tumor microenvironment

Anti-VEGF therapy in addition to RT may enhance anticancer immune response by normalizing tumor vasculature and reprogramming the tumor microenvironment to an immune-permissive status. As shown in Fig. 1b, c, anti-VEGF therapy alone did not significantly alter the expression of PD-1 or PD-L1 on tumor cells or in the microenvironment, as compared to the control group. Combination of anti-VEGF therapy and high-dose ablative irradiation did not show any significant alteration in RT-induced PD-L1 or PD-1 expression on tumor cells or microenvironment components including dendritic cells, MDSCs, and macrophages. Interestingly, when anti-VEGF therapy was administered along with RT, PD-1 expression on CD8+ ($p=0.026$) and CD4+ T cells ($p=0.016$) tended to decrease, implying a insignificant reversal of the immune-suppressive environment.

Tumor vasculature response to RT and anti-VEGF therapy

To assess tumor vasculature response to RT and anti-VEGF therapy, we examined tumor vasculature before RT and 0, 3, 6, 9 days post-RT by quantified power Doppler sonography (Fig. 2a). As shown in Fig. 2b, c, the color density of pixel levels, as compared to the control group, insignificantly decreased at 3 days ($p=0.034$) and 6 days ($p=0.024$) after RT, and recovered 1 week after RT. This indicates that RT causes transient vessel collapse leading to mildly diminished blood flow within 6 days after RT, after which the blood flow is restored. The blood flow assessment results of the combinatorial anti-VEGF therapy + RT group is similar to that in the control group, suggesting that the combinatorial anti-VEGF therapy restores the RT-induced transient vasculature obliteration with preserved tumor blood flow. Moreover, the ultrasonic contrast imaging using microbubble agents was performed before RT, 3 and 9 days post-RT, with MIP demonstrating the path of microbubbles throughout the tumor summation over time (Fig. 2d, e). Varying blood flow summation without statistical difference was observed between groups, suggesting that even if RT incidentally diminished the blood flow, the combinatorial anti-VEGF therapy may restore the tumor blood flow.

Potential anticancer effect of RT, anti-VEGF, and anti-PD-L1 therapy in antitumor immunity

Irradiation-induced upregulation of PD-L1 can provide an opportunity for PD-L1 blockade that would uncover the full cytotoxic potential of host immunity against the tumor. Anti-angiogenic therapy would strengthen the efficacy of immunotherapy as low immune cell infiltration represents a major obstacle for cancer immunotherapy. Whether the trimodal approach, combining RT with anti-angiogenic therapy and immunotherapy, is a promising therapeutic strategy requires further investigation. Therefore, LLC cells were implanted, and the tumor-bearing mice were treated with anti-VEGF, anti-PD-L1, high-dose ablative irradiation (RT, 40 Gy/4 fx on day 1, 2, 3, 4), RT + anti-VEGF, RT + anti-PD-L1, or trimodal combination of RT + anti-PD-L1 + anti-VEGF therapies (Fig. 3a). Noteworthy, the bimodal and trimodal therapies administered in the study were well tolerated without significant adverse effects. Irradiation alone, or in combination with anti-PDL1 and/or anti-VEGF therapies, significantly slowed the tumor progression (Fig. 3b). On day 29, mice treated with irradiation, with or without other treatments, had significantly smaller tumor volumes ($p<0.01$),

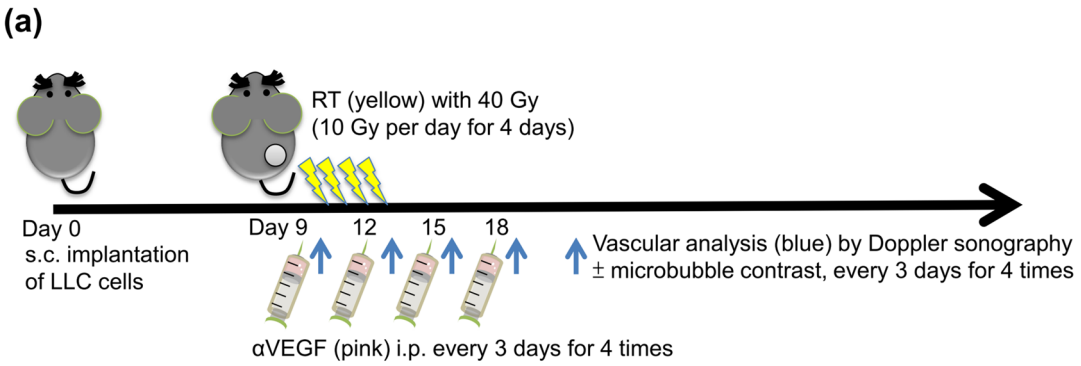
(a)
RT (yellow) with 40 Gy
(10 Gy per day for 4 days)
Day 0
s.c. implantation
of LLC cells
Day 9
12
15
18
Vascular analysis (blue) by Doppler sonography
± microbubble contrast, every 3 days for 4 times
αVEGF (pink) i.p. every 3 days for 4 times

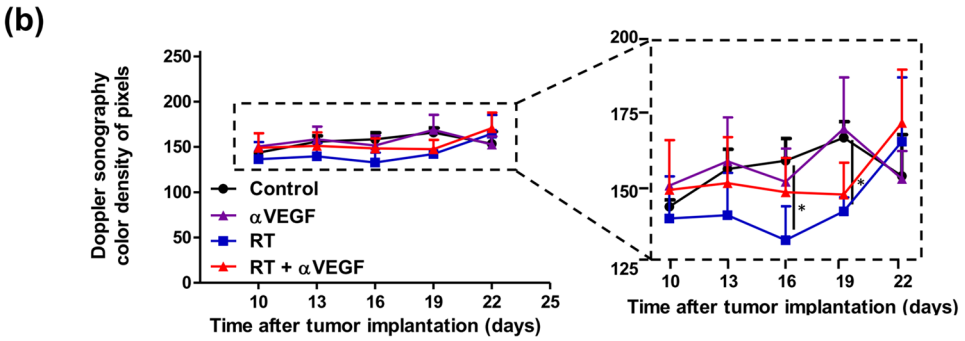
(b)
Doppler sonography
color density of pixels
Control
αVEGF
RT
RT + αVEGF
Time after tumor implantation (days)
Time after tumor implantation (days)

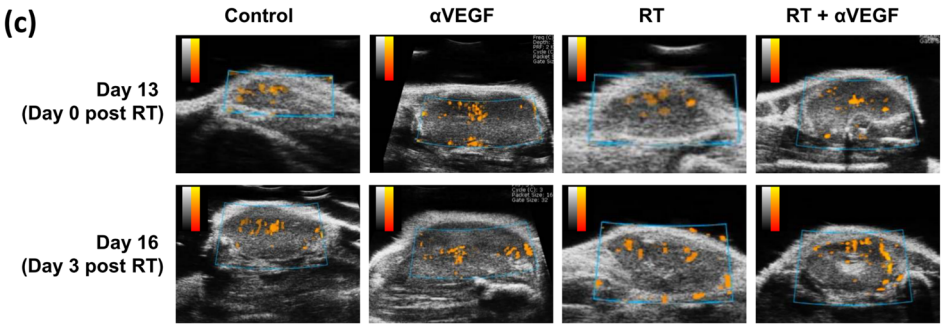
(c)
Control
αVEGF
RT
RT + αVEGF
Day 13
(Day 0 post RT)
Day 16
(Day 3 post RT)

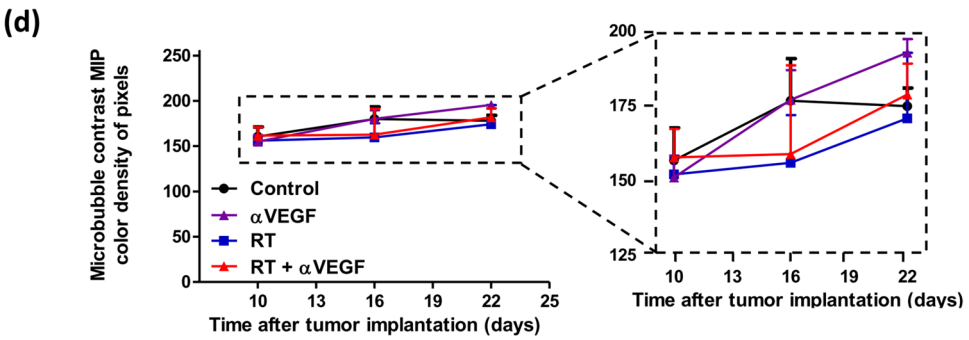
(d)
Microbubble contrast MIP
color density of pixels
Control
αVEGF
RT
RT + αVEGF
Time after tumor implantation (days)
Time after tumor implantation (days)

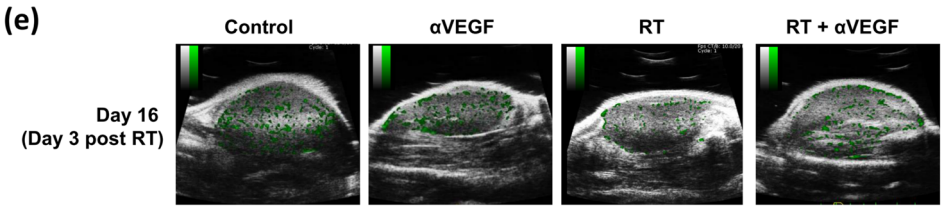
(e)
Control
αVEGF
RT
RT + αVEGF
Day 16
(Day 3 post RT)

◂**Fig. 2** Tumor vasculature response to radiotherapy (RT) and anti-VEGF therapy. **a** C57BL/6 mice were subcutaneously injected into the flank with 2×10^5 LLC cells. Once the tumor was established, mice were locally treated with 10-Gy dose/fraction of RT, one fraction per day, for 4 days, to a total dose of 40 Gy, and 100 μg anti-VEGF was administered intraperitoneally every 3 days for a total of four times. To assess tumor vasculature response to RT and anti-VEGF therapy, quantified power Doppler sonography was performed before RT and 0, 3, 6, and 9 days after RT, to assess vasculature response to RT (40 Gy) and anti-VEGF therapy. Ultrasonic contrast imaging using microbubble agents was performed before RT, as well as 3 and 9 days after RT, with maximal intensity projection (MIP) demonstrating the path of microbubbles throughout the tumor summation over time. The mean color density of pixel levels (**b**) and graphic representation (**c**) of power Doppler sonography; and mean color density of pixel levels (**d**) and graphic representations (**e**) of ultrasonic contrast imaging MIP from the control and treated mice are shown at the indicated time points. The color density of pixel levels ranged from 0 to 255. Higher values indicate more blood flow. $^*p<0.05$

as compared to those in the non-RT groups. On day 53, as compared to the RT alone group, RT + anti-VEGF therapy did not synergistically control the tumor growth ($p=0.261$). Compared to the RT alone group, bimodal therapies of RT + anti-PDL1 therapy achieved significant tumor suppression efficacy ($p=0.008$; Fig. 3b) and showed a trend toward improved survival ($p=0.014$; log-rank Mantel–Cox test; Fig. 3c). When anti-VEGF therapy was combined with RT + anti-PDL1 therapy, similar and more prominent effects were observed along with effective tumor suppression ($p=0.007$) and significantly improved survival ($p=0.003$; Fig. 3c).

Assessment of prolonged protective antitumor immunity after RT, anti-PD-L1, and anti-VEGF therapies

To address whether radiotherapy, anti-PD-L1 therapy, and anti-VEGF therapy results in the generation of prolonged protective T cell immunity, mice were rechallenged with a two-times higher dose of LLC cells (4×10^5 cells) on the opposite flank on day 40. Since mice in the control, anti-PD-L1 alone, and anti-VEGF alone groups met humane endpoints between day 22 and day 31 after tumor implantation, rechallenge experiments at day 40 were not possible in the above-mentioned groups. At day 15 after rechallenge, compared to the RT alone group, bimodal therapies of RT + anti-PD-L1 treatment suppressed the contralateral tumor growth ($p=0.005$, Fig. 4a) showing a trend toward improved survival ($p=0.039$, log-rank Mantel–Cox test, Fig. 4b). Similar and more prominent effect, with delayed growth of contralateral flank tumor after rechallenge ($p=0.002$, Fig. 4a) and significantly improved survival ($p=0.003$, log-rank Mantel–Cox test, Fig. 4b), was observed in the trimodal combination of RT + anti-PD-L1 + anti-VEGF therapies, compared to that in the RT alone group. RT + anti-PD-L1 with or without anti-VEGF therapies led to the prolonged protective T cell immunity, and most of the mice showed no tumor growth after being rechallenged (60% in RT + anti-PD-L1 + anti-VEGF group vs. 50% in RT + anti-PD-L1 group vs. 0% in the RT alone group).

Potential effects of RT, anti-PD-L1, and anti-VEGF therapies on tumor microenvironment

To determine whether the antitumor effect depends on the alteration of tumor microenvironment, we examined the proportion of immune cell populations in the peripheral TILs after treatment. Ten days after irradiation, cells infiltrating the tumors and microenvironments were removed to obtain cell suspensions for surface staining. Anti-VEGF alone, or anti-PD-L1 alone did not significantly alter microenvironmental components compared to the control group. Meanwhile, irradiation (alone or in combination with other modalities) decreased the proportion of dendritic cells, compared to the control group ($p<0.01$, Fig. 5a). Ten days after the irradiation and treatments, bimodal approach of RT + anti-PD-L1 showed a trend toward an increase in the percentage of CD8+ T cells ($p=0.019$, Fig. 5a, b) and a decrease in MDSCs ($p=0.040$, Fig. 5a, c), compared to that in the RT alone group. Furthermore, a parallel and prominent effect was seen in the trimodal combination of RT + anti-PD-L1 + anti-VEGF therapies, with significant increase in the percentage of CD8+ T cells ($p=0.002$, Fig. 5a, b), and significant decrease in MDSCs ($p=0.003$, Fig. 5a, c). The percentage of macrophages was unaffected between the groups. The regulatory T cells were defined as CD25+ and FoxP3+, the percentage of which within the CD4+ T cell population, was also unaffected (Supplementary Fig. 1) between groups. The local accumulation of CD8+ T cells and reduction in MDSCs in the tumor microenvironment may be essential for the therapeutic efficacy of the combination of RT, anti-PD-L1, and anti-VEGF therapies.

Evaluation of memory T cells in TILs and splenocytes after RT, anti-PD-L1, and anti-VEGF therapies

To determine whether RT, anti-PD-L1, and anti-VEGF therapies were associated with induction of memory T cells, these cells in the TILs and splenocytes were quantified (Fig. 6). Naive T cells were defined as CD62L+ and CD44−, effector memory T cells as CD62− and CD44+, and central memory T cells as CD62+ and CD44+ [35]. Compared to the control group, any treatment, including RT, anti-PD-L1, and anti-VEGF therapies, alone or in combination with other treatments, increased the percentage of effector memory T cells ($p<0.01$, Fig. 6a–d), in both TILs and splenocytes. However, although the central memory T cell components

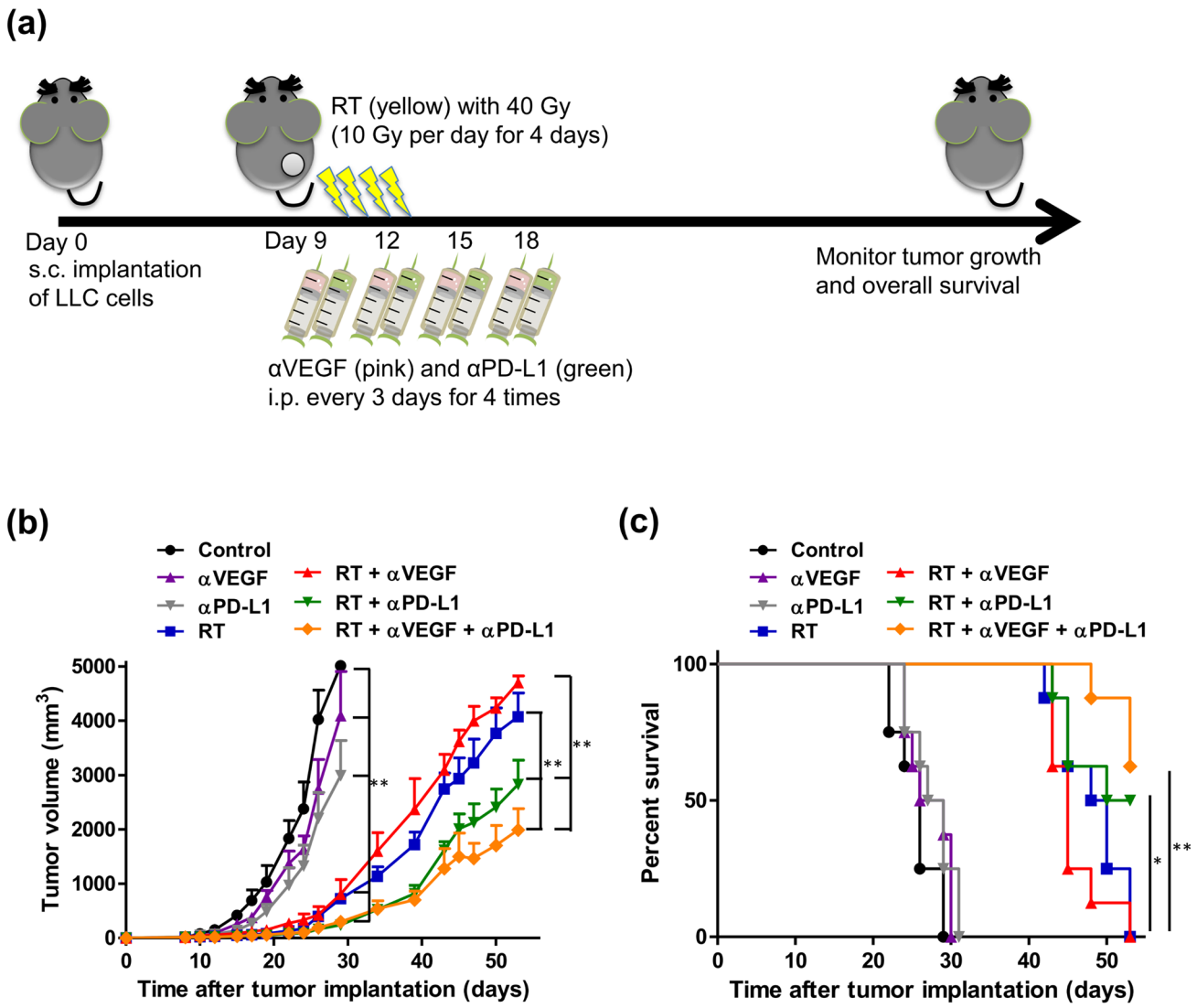

Fig. 3 Potential anti-cancer effects of combining radiotherapy (RT), anti-VEGF, and anti-PD-L1 therapies. C57BL/6 mice were subcutaneously injected into the flank with 2×10^5 LLC cells. At 9 days after tumor implantation, the tumor-bearing mice were randomized into seven treatment groups: control, anti-VEGF (100 μg on day 0, 3, 6, and 9; total 400 μg), anti-PD-L1 (100 μg on day 1, 4, 7, and 10; total 400 μg), RT (40 Gy/4 fx on day 1, 2, 3, and 4), RT + anti-VEGF, RT + anti-PD-L1, and RT + anti-PD-L1 + anti-VEGF, as the scheme shown in **a**. Tumor growth curves (**b**) and survival curves (**c**) in different treatment groups. Data are means ± SEM measured on the indicated days. $^*p<0.05$ and $^{**}p<0.01$. Experimental groups contained five mice per group. Studies were conducted twice in two independent experiments with an interval of 1 month, and the presented data are the combined data of the two independent experiments

did not differ between groups in TILs, an increased proportion of central memory T cells in splenocytes ($p<0.01$, Fig. 6c, d) was observed with irradiation alone or in combination with other treatments. Meanwhile, anti-VEGF alone or anti-PD-L1 alone did not significantly alter the central memory components in splenocytes, compared to the control group. Taken together, the datasets support the concept that anti-cancer treatments increase the proportion of effector memory T cells in TILs and splenocytes, and irradiation, alone or in combination with other treatments, further increases the central memory T cells in splenocytes.

Discussion

Development of novel approaches for the treatment of advanced lung cancer is of paramount importance. Herein, we show that high-dose irradiation alone prompts adaptive responses in tumor cells and in the microenvironment, with upregulation of PD-L1/PD-1 expression on tumor cells and microenvironments leading to subsequent radioresistance; incorporating anti-VEGF therapy with high-dose ablative irradiation insignificantly reverses the immune-suppressive microenvironment. Using a lung cancer mouse model,

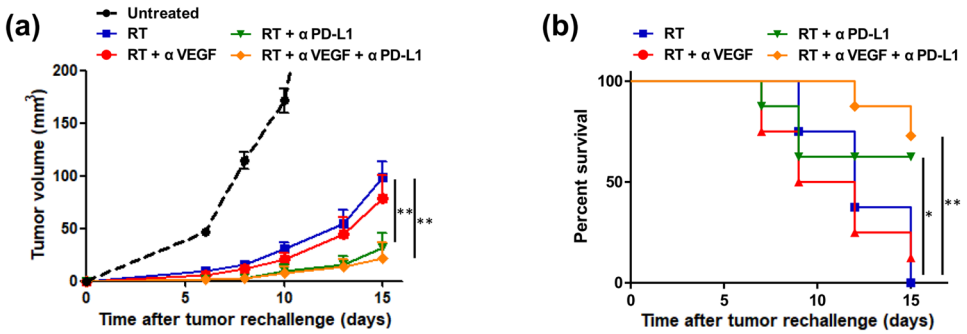

Fig. 4 Assessment of prolonged protective antitumor immunity after radiotherapy (RT), anti-PD-L1, and anti-VEGF therapies. Mice were rechallenged with two-fold higher dose of Lewis lung carcinoma (LLC) cells (4×10^5 cells) on the opposite flank on day 40. The growth curve of 4×10^5 cells injected in the untreated mice was measured as reference. Tumor growth curves (**a**) and survival curves (**b**) in different treatment groups are plotted. Data represent means ± SEM measured on the indicated days. $*p<0.05$ and $**p<0.01$. Experimental groups contained five mice per group. Studies were conducted twice in two independent experiments with an interval of 1 month, and the presented data are the combined data of the two independent experiments

we demonstrated that the efficacy of RT can be enhanced through the combination of anti-PD-L1, leading to the generation of immune memory in mice capable of protecting against tumor recurrence. Combining anti-VEGF therapy with high-dose irradiation and anti-PD-L1 therapy more prominently benefits the existing anti-cancer efficacy.

The LLC mouse syngeneic tumor model was used in the current study, which was established from a tumor on the lung of one C57BL mouse [35] and can be employed as an orthotopic or subcutaneous model, with the latter considered to be the more common. This subcutaneous model offers the ability to, readily establish tumors in immunocompetent hosts, profile tumor infiltrating lymphocytes and microenvironments, and investigate the mechanisms associated with the efficacy of immune-oncology treatments [13, 26]. Therefore, the LLC mouse syngeneic tumor model is adequate for studying the trimodal combination therapy of RT, anti-PD-L1, and anti-angiogenic treatment in our experiments.

While investigating the effect of ablative RT on tumor vasculature, Kim et al. found that treatment of LLC tumors in C57BL/6 mice hind limbs with ablative dose (20 Gy in one fraction) results in transient reduction in, and subsequent recovery of, tumor blood flow 4 days after RT [16], which is in accordance with our results that RT might cause transient vessel collapse with decreased blood flow within the days after ablative irradiation, and subsequent restoration of blood flow. Additionally, in support of our results demonstrating that treatment with anti-VEGF therapy before ablative RT may normalize tumor vasculature and enhance the radiation response, Chauhan et al. have reported that anti-VEGF signaling creates a morphologically and functionally normalized vascular network with the remaining vessels, resulting in improved penetration of drug particles into the tumor [37]. Furthermore, Winkler et al. have demonstrated that anti-VEGF therapy before ablative RT creates a normalization window on orthotopic U87 gliomas characterized by a decrease in tumor hypoxia and an increase in tumor oxygenation with enhanced radiation response [17].

PD-L1 has been found to be expressed on macrophages, dendritic cells and MDSCs in response to antigens and stimulating factors, on T cells and B cells upon receptor signaling, and on murine tumor cell lines, while PD-1 is expressed on the surface of activated T cells, B cells, and macrophages [36–38]. In line with these findings, our results showed expression of PD-L1 and PD-1 on tumor and microenvironment cells, while the highly expressed PD-1 was observed following irradiation on T cells, B cells, and macrophages (shown by median fluorescence intensity in Fig. 1c), suggesting negative regulation of the immune responses upon ablative irradiation.

In our study, RT + anti-PD-L1 therapy resulted in prolonged protective antitumor immunity in the rechallenge experiments, while combining anti-VEGF and RT + anti-PD-L1 therapies augmented the existing antitumor immunity. Double tumor cell numbers were used for these experiments to confirm the development of a long-lived immune memory against tumor antigens, resulting in tumor rejection and preventing growth of rechallenged tumor cells [6, 39]. The murine monoclonal antibody, IgG2b, has a serum half-life of 4–6 days, as determined by enzyme-linked immunosorbent assay (ELISA). At the day of rechallenge (day 40), the serum concentration of murine monoclonal antibodies was diminished to 100–1000 times lower than the initial serum concentrations, thus it can be assumed that no antibody activity was detectable [40, 41].

According to our results, local accumulation of CD8+ T cells and reduction in MDSCs in the tumor microenvironment may be essential for the therapeutic efficacy of the combination of RT, anti-PD-L1, and anti-VEGF therapies, without altering the CD4+ T cell population or the

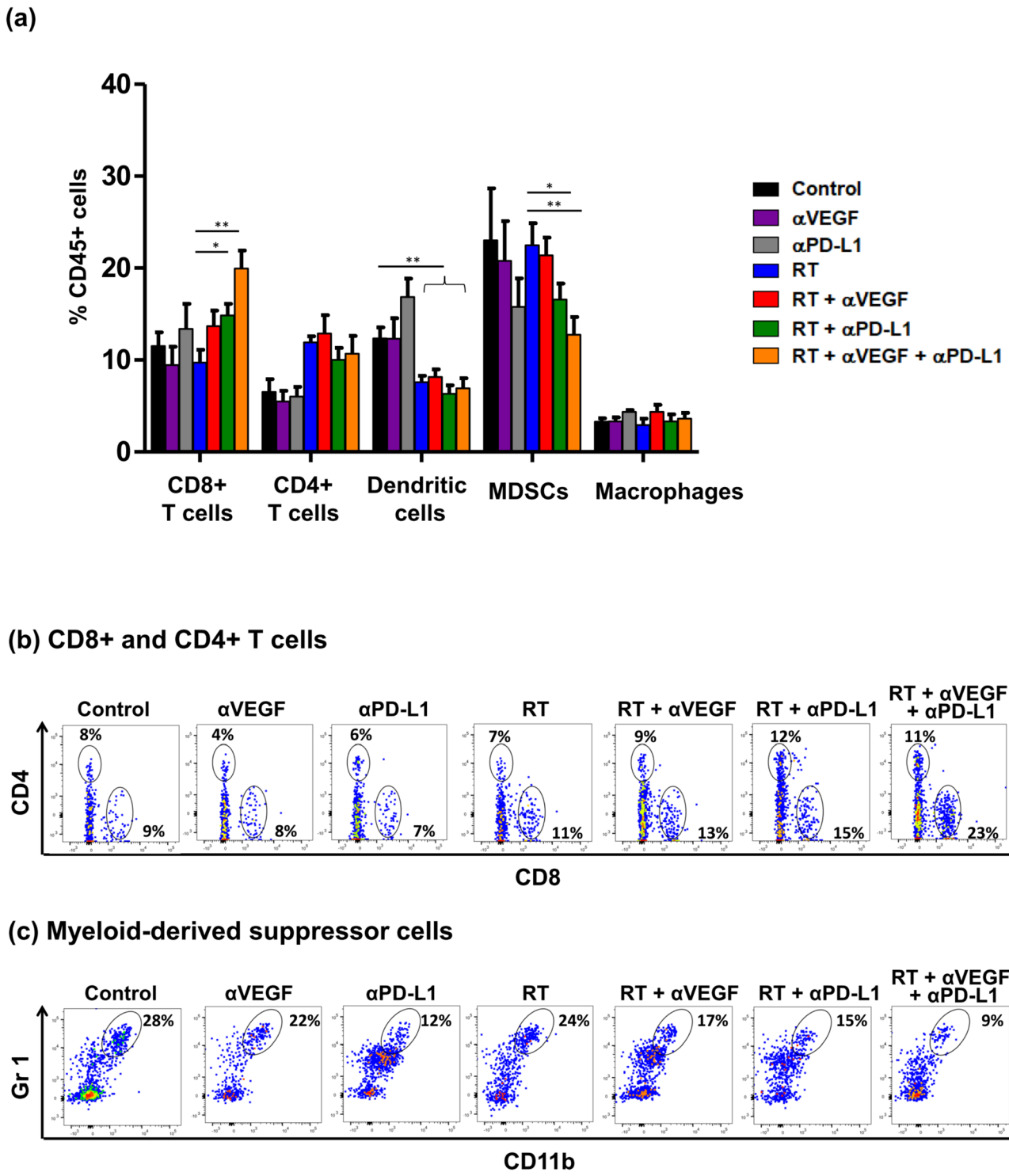

regulatory T cell subpopulation. The CD4+ T cell population contains effector T cells and Tregs, which can function as immune stimulators and immune suppressors, respectively. In previous studies, although CD4+ T cells can mediate the cytotoxic function against tumor cells when combining RT and anti-PD-L1 therapies, CD4+ T cells were observed to be dispensable during the priming process [6], likely explained by both effector CD4+ T cells and regulatory CD4+ T cells, given the presumed opposing roles of each [11]. Yet, further studies are needed to evaluate the relative contributions of the subpopulations of CD4+ T cells. On the other hand, MDSCs have been shown to suppress T cell activation, promote tumor outgrowth, and alter the tumor immune microenvironment. In a previous study [6],

◂**Fig. 5** Influence of radiotherapy (RT), anti-PD-L1, and anti-VEGF therapies on T cells and myeloid-derived suppressor cells (MDSCs). C57BL/6 mice were subcutaneously injected into the flank with 2×10^5 LLC cells. At 9 days after tumor implantation, the tumor-bearing mice were randomized into seven treatment groups: control, anti-VEGF (100 μg on day 0, 3, 6, and 9; total 400 μg), anti-PD-L1 (100 μg on day 1, 4, 7, and 10; total 400 μg), RT (40 Gy/4 fx on day 1, 2, 3, and 4), RT + anti-VEGF, RT + anti-PD-L1, and RT + anti-PD-L1 + anti-VEGF. Ten days after RT, infiltrating cells in the tumor microenvironments were removed to obtain cell suspensions for surface staining. **a** Quantitative data representing the proportion of CD8+ T cells, CD4+ T cells, dendritic cells, myeloid-derived suppressor cells (MDSCs, CD11b+Gr1+), and macrophages relative to CD45+ cells 10 days after administration of the RT dose. Data represent means ± SEM. Flow cytometric analysis of CD8+ T cells, CD4+ T cells (**b**), and MDSCs (**c**) gated on CD45+ cells in tumors ten days after RT. $*p<0.05$ and $**p<0.01$. Experimental groups contained five mice per group. Studies were conducted twice in two independent experiments with an interval of 1 month, and the presented quantitative histograms (**a**) are the combined data of the two independent experiments

the combination of irradiation and anti-PD-L1 resulted in the elimination of MDSCs from the tumor microenvironment, with the associated mechanism between TNF or FAS/FASL pathway, which is in line with our results.

Anti-VEGF therapy, in combination with cancer immunotherapy, has promising results in both preclinical and clinical setting. Combined anti-VEGF and PD-L1 blockade displayed a synergistic treatment effect in a mouse model of small cell lung cancer, in which the tumor-associated PD-1/TIM-3 double positive T cell phenotype was abrogated by addition of anti-VEGF treatment with anti-PD-L1 [42]. Recently, in patients with metastatic renal cell carcinoma, anti-VEGF therapy in combination with anti-PD-L1 treatments prolonged the progression-free survival with a favorable safety profile [21]. These results support the use of the combination of anti-VEGF therapy and cancer immunotherapy as a first-line treatment option for selected patients.

The trimodal approach of combining RT, anti-PD-L1, and anti-VEGF therapies is under investigation in both preclinical and clinical setting. The trimodal strategy (RT, anti-PD-L1, and anti-VEGF) showed similar but more prominent antitumor immunity than that of the bimodal strategy (RT and anti-PD-L1). Our preclinical results, however, demonstrated no significant benefits when anti-VEGF was combined with RT and anti-PD-L1 therapies, which implied an additive, rather than synergistic, antitumor immunity. Furthermore, in the patients with recurrent high-grade glioma, the phase I trial for trimodal combination of PD-1 blockade with RT and anti-angiogenic therapy was generally well tolerated, and half of the patients achieved durable objective response [25]. Thus, clinical investigation of the trimodal combination therapy is encouraging [24].

The RT dose and its fractionation influence the phenotype and antitumor activity in the immune response. Several preclinical studies have demonstrated the superiority of hypofractionated ablative doses (≥ 10 Gy per fraction for a total dose of 10–50 Gy) on the generation of antitumor response, while ablative tumor radiation transforms the immunosuppressive tumor microenvironment into one that is proimmunogenic, resulting in significant infiltration of CD8+ T cells and a loss of MDSCs, which agrees with our results [4–6]. In clinical practice, ablative radiation achieved by hypofractionation (40–50 Gy in 4–5 fractions) has proven promising when incorporated into therapeutic regimens for early-stage lung cancer and lung oligometastases [7, 8]. Therefore, in the present study, we administered ablative dose fractionation to achieve adequate immunogenicity response. We observed that ablative RT triggers PD-L1 expression in tumor microenvironments within 3 days of RT, which remained elevated for more than one week, accompanied with elevated PD-1 expression on tumor-infiltrating CD4+ and CD8+ T cells. Ablative RT doses have been shown to increase both tumor cells and microenvironment PD-L1-related expression [6]. Clinical trials using ablative RT in combination with anti-PD-1 or anti-PD-L1 therapy are underway.

This study describes a novel anticancer strategy using high-dose irradiation in combination with anti-PD-L1 and anti-angiogenic therapies. Although our findings did not show outstanding benefits of combining anti-VEGF with ablative RT and anti-PD-L1 therapies, they indeed implied an additive, rather than synergistic, antitumor immunity. These results still broaden the scope of current endeavors for operating the immunosuppressive tumor microenvironment and should provide insights into the design of new combination treatments.

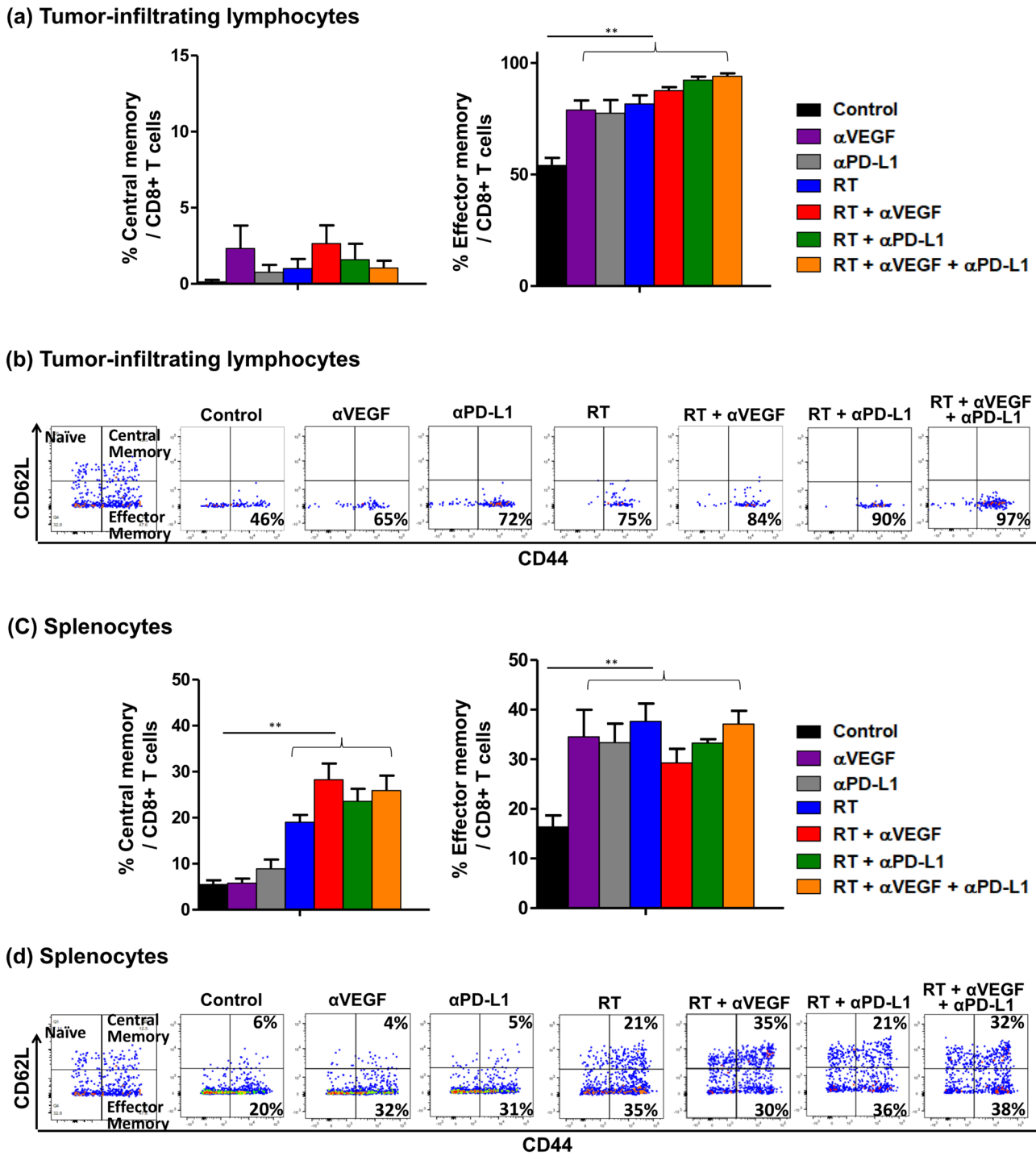

Fig. 6 Evaluation of memory T cells in tumor-infiltrating lymphocytes (TILs) and splenocytes after radiotherapy (RT), anti-PD-L1, and anti-VEGF therapies. C57BL/6 mice were subcutaneously injected into the flank with 2×10^5 LLC cells. At 9 days after tumor implantation, the tumor-bearing mice were randomized into seven treatment groups: control, anti-VEGF (100 μg on day 0, 3, 6, and 9; total 400 μg), anti-PD-L1 (100 μg on day 1, 4, 7, and 10; total 400 μg), RT (40 Gy/4 fx on day 1, 2, 3, and 4), RT + anti-VEGF, RT + anti-PD-L1, and RT + anti-PD-L1 + anti-VEGF. Ten days after RT, infiltrating lymphocytes were isolated from the tumor microenvironments and spleen to obtain cell suspensions for surface staining. Quantitative data for the proportions of the various memory T cell populations in TILs (**a**) and in the spleen (**c**). Flow cytometric analysis of memory markers on CD8+ T cells isolated from TILs (**b**) and spleen (**d**). Data represent means ± SEM measured. $^{**}p<0.01$. Experimental groups contained five mice per group. Studies were conducted twice in two independent experiments with an interval of 1 month, and the presented quantitative histograms (**a**) and (**c**) are the combined data of the two independent experiments

Acknowledgements This study was presented in part at the Radiological Society of North America 104th Scientific Assembly and Annual Meeting (Chicago, USA, November 2019). We thank the staff of the Core Labs, Department of Medical Research, National Taiwan University Hospital, for their technical support.

Author contributions JLYC, CKP, and YLL conceived and designed the experiments. JLYC, YSH, CKP, CYT, and YLL conducted the experiments. JLYC, CKP, and CWW interpreted the results of the experiments. JLYC, YSH, CWW, and YLL drafted and edited the manuscript. SHK and MJS supervised the study. All authors have read and approved the final version of the manuscript.

Funding This work was supported by the National Taiwan University Hospital (Grant numbers NTUH 107-N4008, 108-N4353, and 109-N4547) and the Ministry of Science and Technology (MST, Taiwan, Contract No. MST 106-2314-B-002-052-MY2).

Code availability Not applicable.

Compliance with ethical standards

Conflict of interest The authors declare that they have no competing interests.

Ethics approval All in vivo experimental protocols were approved by the Institutional Animal Care and Use Committee (IACUC 20160399). Humane endpoints were determined according to a clinical scoring system based on that outlined by the IACUC of our institution.

Consent to participate Not applicable.

Consent for publications Not applicable.

Availability of data ad material All data generated and analyzed during this study are included in this published article (and its supplementary information files).

References

1. Citrin DE (2017) Recent developments in radiotherapy. N Engl J Med 377:1065–1075. https://doi.org/10.1056/NEJMra1608986
2. Demaria S, Golden EB, Formenti SC (2015) Role of local radiation therapy in cancer immunotherapy. JAMA Oncol 1:1325–1332. https://doi.org/10.1001/jamaoncol.2015.2756
3. Formenti SC, Demaria S (2013) Combining radiotherapy and cancer immunotherapy: a paradigm shift. J Natl Cancer Inst 105:256–265. https://doi.org/10.1093/jnci/djs629
4. Filatenkov A, Baker J, Mueller AM et al (2015) Ablative tumor radiation can change the tumor immune cell microenvironment to induce durable complete remissions. Clin Cancer Res 21:3727–3739. https://doi.org/10.1158/1078-0432.ccr-14-2824
5. Lee Y, Auh SL, Wang Y et al (2009) Therapeutic effects of ablative radiation on local tumor require CD8+ T cells: changing strategies for cancer treatment. Blood 114:589–595. https://doi.org/10.1182/blood-2009-02-206870
6. Deng L, Liang H, Burnette B, Beckett M, Darga T, Weichselbaum RR, Fu YX (2014) Irradiation and anti-PD-L1 treatment synergistically promote antitumor immunity in mice. J Clin Invest 124:687–695. https://doi.org/10.1172/jci67313
7. Baumann P, Nyman J, Hoyer M et al (2009) Outcome in a prospective phase II trial of medically inoperable stage I non-small-cell lung cancer patients treated with stereotactic body radiotherapy. J Clin Oncol 27:3290–3296. https://doi.org/10.1200/jco.2008.21.5681
8. Palma DA, Olson R, Harrow S et al (2019) Stereotactic ablative radiotherapy versus standard of care palliative treatment in patients with oligometastatic cancers (SABR-COMET): a randomised, phase 2, open-label trial. Lancet 393:2051–2058. https://doi.org/10.1016/s0140-6736(18)32487-5
9. Pennock GK, Chow LQ (2015) The evolving role of immune checkpoint inhibitors in cancer treatment. Oncologist 20:812–822. https://doi.org/10.1634/theoncologist.2014-0422
10. Lim YJ, Koh J, Kim K et al (2015) High ratio of programmed cell death protein 1 (PD-1)(+)/CD8(+) tumor-infiltrating lymphocytes identifies a poor prognostic subset of extrahepatic bile duct cancer undergoing surgery plus adjuvant chemoradiotherapy. Radiother Oncol 117:165–170. https://doi.org/10.1016/j.radonc.2015.07.003
11. Dovedi SJ, Adlard AL, Lipowska-Bhalla G et al (2014) Acquired resistance to fractionated radiotherapy can be overcome by concurrent PD-L1 blockade. Cancer Res 74:5458–5468. https://doi.org/10.1158/0008-5472.can-14-1258
12. Mowery YM, Patel K, Chowdhary M et al (2019) Retrospective analysis of safety and efficacy of anti-PD-1 therapy and radiation therapy in advanced melanoma: a bi-institutional study. Radiother Oncol 138:114–120. https://doi.org/10.1016/j.radonc.2019.06.013
13. Lin H, Wei S, Hurt EM et al (2018) Host expression of PD-L1 determines efficacy of PD-L1 pathway blockade-mediated tumor regression. J Clin Invest 128:805–815. https://doi.org/10.1172/jci96113
14. Lee CG, Heijn M, di Tomaso E et al (2000) Anti-vascular endothelial growth factor treatment augments tumor radiation response under normoxic or hypoxic conditions. Cancer Res 60:5565–5570
15. Timke C, Zieher H, Roth A, Hauser K, Lipson KE, Weber KJ, Debus J, Abdollahi A, Huber PE et al (2008) Combination of vascular endothelial growth factor receptor/platelet-derived growth factor receptor inhibition markedly improves radiation tumor therapy. Clin Cancer Res 14:2210–2219. https://doi.org/10.1158/1078-0432.CCR-07-1893
16. Kim DW, Huamani J, Niermann KJ, Lee H, Geng L, Leavitt LL, Baheza RA, Jones CC, Tumkur S, Yankeelov TE, Fleischer AC, Hallahan DE (2006) Noninvasive assessment of tumor vasculature response to radiation-mediated, vasculature-targeted therapy using quantified power Doppler sonography: implications for improvement of therapy schedules. J Ultrasound Med 25:1507–1517. https://doi.org/10.7863/jum.2006.25.12.1507
17. Winkler F, Kozin SV, Tong RT et al (2004) Kinetics of vascular normalization by VEGFR2 blockade governs brain tumor response to radiation: role of oxygenation, angiopoietin-1, and matrix metalloproteinases. Cancer Cell 6:553–563. https://doi.org/10.1016/j.ccr.2004.10.011
18. Folkman J (1971) Tumor angiogenesis: therapeutic implications. N Engl J Med 285:1182–1186. https://doi.org/10.1056/nejm197111182852108
19. Ott PA, Hodi FS, Buchbinder EI (2015) Inhibition of immune checkpoints and vascular endothelial growth factor as combination therapy for metastatic melanoma: an overview of rationale, preclinical evidence, and initial clinical data. Front Oncol 5:202. https://doi.org/10.3389/fonc.2015.00202
20. Fukumura D, Kloepper J, Amoozgar Z, Duda DG, Jain RK (2018) Enhancing cancer immunotherapy using antiangiogenics: opportunities and challenges. Nat Rev Clin Oncol 15:325–340. https://doi.org/10.1038/nrclinonc.2018.29
21. Rini BI, Powles T, Atkins MB et al (2019) Atezolizumab plus bevacizumab versus sunitinib in patients with previously untreated metastatic renal cell carcinoma (IMmotion151): a multicentre,

open-label, phase 3, randomised controlled trial. Lancet 393:2404–2415. https://doi.org/10.1016/s0140-6736(19)30723-8
22. Shrimali RK, Yu Z, Theoret MR, Chinnasamy D, Restifo NP, Rosenberg SA (2010) Antiangiogenic agents can increase lymphocyte infiltration into tumor and enhance the effectiveness of adoptive immunotherapy of cancer. Cancer Res 70:6171–6180. https://doi.org/10.1158/0008-5472.can-10-0153
23. Finn RS, Qin S, Ikeda M et al (2020) Atezolizumab plus bevacizumab in unresectable hepatocellular carcinoma. N Engl J Med 382:1894–1905
24. Goedegebuure RSA, de Klerk LK, Bass AJ, Derks S, Thijssen VLJL (2019) Combining radiotherapy with anti-angiogenic therapy and immunotherapy: a therapeutic triad for cancer? Front Immunol 9:3107. https://doi.org/10.3389/fimmu.2018.03107
25. Sahebjam S, Forsyth P, Arrington J et al (2017) ATIM-18. A phase I trial of hypofractionated stereotactic irradiation (HFSRT) with pembrolizumab and bevacizumab in patients with recurrent high grade gliomas (NCT02313272). Neuro-Oncol 18:vi21. https://doi.org/10.1093/neuonc/nox168.113
26. Li QX, Feuer G, Ouyang X, An X (2017) Experimental animal modeling for immuno-oncology. Pharmacol Ther 173:34–46. https://doi.org/10.1016/j.pharmthera.2017.02.002
27. Twyman-Saint Victor C, Rech AJ, Maity A et al (2015) Radiation and dual checkpoint blockade activate non-redundant immune mechanisms in cancer. Nature 520:373–377. https://doi.org/10.1038/nature14292
28. Ngiow SF, Young A, Jacquelot N, Yamazaki T, Enot D, Zitvogel L, Smyth MJ (2015) A threshold level of intratumor CD8+ T-cell PD1 expression dictates therapeutic response to anti-PD1. Cancer Res 75:3800–3811. https://doi.org/10.1158/0008-5472.can-15-1082
29. Chen YF, Yuan A, Cho KH, Lu YC, Kuo MY, Chen JH, Chang YC (2017) Functional evaluation of therapeutic response of HCC827 lung cancer to bevacizumab and erlotinib targeted therapy using dynamic contrast-enhanced and diffusion-weighted MRI. PLoS ONE 12(11):e0187824. https://doi.org/10.1371/journal.pone.0187824
30. Dings RP, Loren M, Heun H, McNiel E, Griffioen AW, Mayo KH, Griffin RJ (2007) Scheduling of radiation with angiogenesis inhibitors anginex and Avastin improves therapeutic outcome via vessel normalization. Clin Cancer Res 13:3395–3402. https://doi.org/10.1158/1078-0432.ccr-06-2441
31. du Manoir JM, Francia G, Man S, Mossoba M, Medin JA, Viloria-Petit A, Hicklin DJ, Emmenegger U, Kerbel RS (2006) Strategies for delaying or treating in vivo acquired resistance to trastuzumab in human breast cancer xenografts. Clin Cancer Res 12:904–916. https://doi.org/10.1158/1078-0432.ccr-05-1109
32. Chen JL-Y, Tsai Y-C, Tsai M-H, Lee S-Y, Wei M-F, Kuo S-H, Shieh M-J (2017) Prominin-1-specific binding peptide-modified apoferritin nanoparticle carrying irinotecan as a novel radiosensitizer for colorectal cancer stem-like cells. Part Part Syst Charact 34:1600424. https://doi.org/10.1002/ppsc.201600424
33. Li X, Zhang R, Li Z et al (2017) Contrast-enhanced ultrasound imaging quantification of adventitial vasa vasorum in a rabbit model of varying degrees of atherosclerosis. Sci Rep 7:7032. https://doi.org/10.1038/s41598-017-06127-w
34. Gates S (2020) Statistical significance and clinical evidence. Lancet Oncol 21:317–466. https://doi.org/10.1016/s1470-2045(19)30854-x
35. Bertram JS, Janik P (1980) Establishment of a cloned line of Lewis lung carcinoma cells adapted to cell culture. Cancer Lett 11:63–73. https://doi.org/10.1016/0304-3835(80)90130-5
36. Freeman GJ, Long AJ, Iwai Y et al (2000) Engagement of the PD-1 immunoinhibitory receptor by a novel B7 family member leads to negative regulation of lymphocyte activation. J Exp Med 192:1027–1034. https://doi.org/10.1084/jem.192.7.1027
37. Yamazaki T, Akiba H, Iwai H et al (2002) Expression of programmed death 1 ligands by murine T cells and APC. J Immunol 169:5538–5545. https://doi.org/10.4049/jimmunol.169.10.5538
38. Blank C, Brown I, Peterson AC, Spiotto M, Iwai Y, Honjo T, Gajewski TF (2004) PD-L1/B7H-1 inhibits the effector phase of tumor rejection by T cell receptor (TCR) transgenic CD8+ T cells. Cancer Res 64:1140–1145. https://doi.org/10.1158/0008-5472.can-03-3259
39. van Elsas A, Hurwitz AA, Allison JP (1999) Combination immunotherapy of B16 melanoma using anti-cytotoxic T lymphocyte-associated antigen 4 (CTLA-4) and granulocyte/macrophage colony-stimulating factor (GM-CSF)-producing vaccines induces rejection of subcutaneous and metastatic tumors accompanied by autoimmune depigmentation. J Exp Med 190:355–366. https://doi.org/10.1084/jem.190.3.355
40. Unverdorben F, Richter F, Hutt M, Seifert O, Malinge P, Fischer N, Kontermann RE (2016) Pharmacokinetic properties of IgG and various Fc fusion proteins in mice. MAbs 8:120–128. https://doi.org/10.1080/19420862.2015.1113360
41. Vieira P, Rajewsky K (1988) The half-lives of serum immunoglobulins in adult mice. Eur J Immunol 18:313–316. https://doi.org/10.1002/eji.1830180221
42. Meder L, Schuldt P, Thelen M et al (2018) Combined VEGF and PD-L1 blockade displays synergistic treatment effects in an autochthonous mouse model of small cell lung cancer. Cancer Res 78:4270–4281. https://doi.org/10.1158/0008-5472.can-17-2176